Fibers and Polymers 2002, Vol.3, No.3, 120-127

Nonsteady Plane-strain Ideal Forming without Elastic Dead-zone

Kwansoo Chung*, Wonoh Lee, Tae Jin Kang, and Jae Ryoun Youn

School of Materials Science and Engineering, Seoul National University, 56-1, Shinlim-dong, Kwanak-ku, Seoul 151-742, Korea

(Received July 9, 2002; Revised August 12, 2002; Accepted August 17, 2002)

Abstract: Ever since the ideal forming theory has been developed for process design purposes, application has been limited to sheet forming and, for bulk forming, to two-dimensional steady flow. Here, application for the non-steady case was made under the plane-strain condition. In the ideal flow, material elements deform following the minimum plastic work path (or mostly proportional true strain path) so that the ideal plane-strain flow can be effectively described using the two-dimensional orthogonal convective coordinate system. Besides kinematics, schemes to optimize preform shapes for a prescribed final part shape and also to define the evolution of shapes and frictionless boundary tractions were developed. Discussions include numerical calculations made for a real automotive part under forging.

Keywords: Rigid-perfect plasticity, Nonsteady bulk forming, Characteristic method, Orthogonal convective coordinate system

Introduction

In order to improve trial-and-error based conventional practices for optimizing forming processes, a direct design theory, called the ideal forming theory, has been previously developed. Early work on this, however, was limited to two-dimensional steady flow of rigid-perfect plastic solids[1-3]. Hill[4], who proposed the name, ideal flow, generalized the effort to three-dimensional steady flow. Further extension to non-steady three-dimensional flow was made by Wienecke and Richmond[5], but without specific application to forming.

For the general ideal flow including work-hardening solids, Chung and Richmond[6] proposed the ideal forming theory in which materials deform following the minimum plastic work path (or mostly the proportional true strain path). Chung and Richmond[7] showed that a special deformation theory of plasticity is derived from the flow theory for such ideal flow. Practical design application for non-steady flow followed mainly for sheet forming without friction[8-11] and also with frictional boundary condition[12].

Here, the ideal forming theory is applied for the non-steady plane-strain case, considering isotropic rigid-perfect plasticity. For such cases, to account for the minimum plastic work condition in the ideal flow, principal stretch lines are materially embedded and its kinematics can be effectively described using the two-dimensional orthogonal convective coordinate system. In this coordinate system, the orthogonal base vectors represent principal directions of deformation, which are materially fixed during ideal flow. A numerical code to generate the orthogonal convective coordinate system was developed based on the characteristic method in this work. Besides kinematics, the equilibrium condition and schemes to optimize preform shapes for a prescribed final part shape and also to define the evolution of shapes and frictionless boundary tractions were established. For demonstration purposes, numerical calculations were made for a real automotive part under forging.

*Corresponding author: chungch@gong.snu.ac.kr

Kinematics

Orthogonal Convective Coordinate System

For Mises isotropic materials, the minimum plastic work path for ideal flow complies with the proportional true strain path[13,14] while, for Tresca materials, the condition requires only the absolute maximum principal line to be materially embedded[15]. Therefore, for the plane-strain ideal flow, two principal stretch lines are materially fixed for both Mises and Tresca cases and its kinematics is effectively described using the orthogonal convective coordinate system: the $\xi-\eta$ principal line system.

In the $\xi-\eta$ coordinate system, which is shown in Figure 1 based on the $x-y$ Cartesian system, the following relationship is obtained for the (covariant) base vectors, g_ξ and g_η:

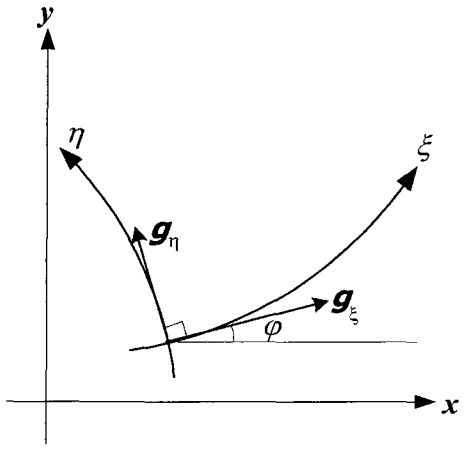

Figure 1. The orthogonal convective $\xi-\eta$ coordinate system.

$$h_\xi = |\boldsymbol{g}_\xi| = (x_{,\xi}^2 + y_{,\xi}^2)^{0.5}$$
$$h_\eta = |\boldsymbol{g}_\eta| = (x_{,\eta}^2 + y_{,\eta}^2)^{0.5}. \quad (1)$$

Note that $\boldsymbol{g}_\xi$ has an angle φ from the x-axis, while $\boldsymbol{g}_\xi$ and $\boldsymbol{g}_\eta$ are orthogonal in Figure 1. As for the local area, it can be assumed to be uniformly unit without losing generality[16]; i.e.,

$$h_\xi h_\eta = 1.0. \quad (2)$$

Conserving the local area as shown in equation (2) also accounts for incompressibility in rigid-plasticity.

Geometric consideration in Figure 1 leads to

$$x_{,\xi} = h\cos\varphi \quad y_{,\xi} = h\sin\varphi$$
$$x_{,\eta} = -\frac{1}{h}\sin\varphi \quad y_{,\eta} = \frac{1}{h}\cos\varphi, \quad (3)$$

where the scaling factor, $h = h_\xi$ and $h_\eta = 1/h$. The compatibility conditions are

$$x_{,\xi\eta} = x_{,\eta\xi} \quad y_{,\xi\eta} = y_{,\eta\xi} \quad (4)$$

and, therefore, the following equations are obtained from equations (3) and (4), after $\varphi = 0.0$ is assumed without losing generality:

$$hh_{,\eta} + \varphi_{,\xi} = 0 \quad h^3\varphi_{,\eta} + h_{,\xi} = 0. \quad (5)$$

Equation (5) shows two partial differential equations for two unknowns, h and φ, which define the orthogonal convective coordinate system having a uniform unit local area.

Characteristic Method

Consider the following second order partial differential equation:

$$\frac{\partial^2\Phi}{\partial\xi^2} - \left(2\frac{\partial\Phi}{\partial\xi}\right)^2\frac{\partial^2\Phi}{\partial\eta^2} = 0, \quad (6)$$

which is the non-linear hyperbolic equation. After applying $v = 2\Phi_{,\xi}$ and $w = \Phi_{,\eta}$, equation (6) becomes

$$\frac{1}{2}\frac{\partial v}{\partial\xi} - v^2\frac{\partial w}{\partial\eta} = 0 \quad \frac{1}{2}\frac{\partial v}{\partial\eta} - \frac{\partial w}{\partial\xi} = 0. \quad (7)$$

Equation (7) is equivalent to equation (5), when $v = h^2$ and $w = -\varphi$. The procedure demonstrates that equation (7) is the quasi-linear hyperbolic equation, which can be solved using the characteristic method. The method provides the following two ordinary differential equations along the characteristic lines, α and β lines, from equation (7):

$$d\ \ln h - d\varphi = 0 \quad \text{for which} \quad \eta_{,\xi} = -h^2 \quad (\alpha-\text{line})$$
$$d\ \ln h + d\varphi = 0 \quad \text{for which} \quad \eta_{,\xi} = h^2 \quad (\beta-\text{line}), \quad (8)$$

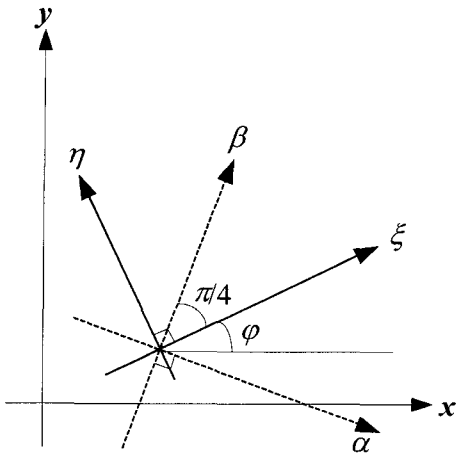

Figure 2. The characteristic (α and β) and principal (ξ and η) lines.

which are expressed in the convective coordinate system.

In order to express the characteristic lines in the $x-y$ coordinate system, consider

$$dx = (x_{,\xi} \pm h^2 x_{,\eta})d\xi = h(\cos\varphi \mp \sin\varphi)d\xi$$
$$dy = (y_{,\xi} \pm h^2 y_{,\eta})d\xi = h(\sin\varphi \pm \cos\varphi)d\xi. \quad (9)$$

The upper and lower signs in equation (9) are valid for the α and β lines, respectively. Therefore,

$$\frac{dy}{dx} = \frac{\sin\varphi - \cos\varphi}{\cos\varphi + \sin\varphi} = \tan\left(\varphi - \frac{\pi}{4}\right) \text{ for the } \alpha \text{ line}$$
$$\frac{dy}{dx} = \frac{\sin\varphi + \cos\varphi}{\cos\varphi - \sin\varphi} = \tan\left(\varphi + \frac{\pi}{4}\right) \text{ for the } \beta \text{ line}, \quad (10)$$

while, for the principal lines,

$$\frac{dy}{dx} = \tan\varphi \quad \text{for the } \xi\text{-line } (d\eta = 0)$$
$$\frac{dy}{dx} = \frac{-1}{\tan\varphi} \quad \text{for the } \eta\text{-line } (d\xi = 0). \quad (11)$$

Equations (8), (10), and (11) show that the characteristic lines are not orthogonal in the $\xi - \eta$ system, but they are orthogonal and located between the principal lines in the $x-y$ coordinate system as shown in Figure 2. Example numerical solutions to construct the orthogonal convective coordinate system under several boundary conditions are elsewhere[17].

Equilibrium Condition

In the two-dimensional space, the equilibrium condition becomes

$$\sigma_{x,x} + \sigma_{xy,y} = 0 \quad \sigma_{xy,x} + \sigma_{y,y} = 0, \quad (12)$$

where σ_x, σ_y and σ_{xy} are the Cartesian Cauchy stress components, while the yield stress condition for the rigid-

perfect plasticity of Mises and Tresca cases is

$$(\sigma_x - \sigma_y)^2 + 4\sigma_{xy}^2 = 4k^2 \tag{13}$$

or

$$\sigma_x = -p \pm k\cos 2\varphi \quad \sigma_y = -p \mp k\cos 2\varphi$$
$$\sigma_{xy} = \pm k\sin 2\varphi \tag{14}$$

where k is the shear yield stress and $p = -(\sigma_x + \sigma_y)/2$. The upper and lower signs in equation (14) are for the cases when $h_\xi > h_\xi^o$ and $h_\xi < h_\xi^o$, respectively, as shown in Figure 3 (here, h_ξ^o is the value at the initial configuration). Note that σ_z is uniquely determined for the Mises case, $\sigma_z = -p = (\sigma_x + \sigma_y)/2 = (\sigma_\xi + \sigma_\eta)/2$, while σ_z is a non-unique value between σ_ξ and σ_η for the Tresca case.

When equation (14) is applied, equation (12) becomes

$$p_{,x} \pm 2k\sin 2\varphi\varphi_{,x} \mp 2k\cos 2\varphi\varphi_{,y} = 0$$
$$p_{,y} \mp 2k\cos 2\varphi\varphi_{,x} \mp 2k\sin 2\varphi\varphi_{,y} = 0 \tag{15}$$

in the $x - y$ coordinate system and this becomes

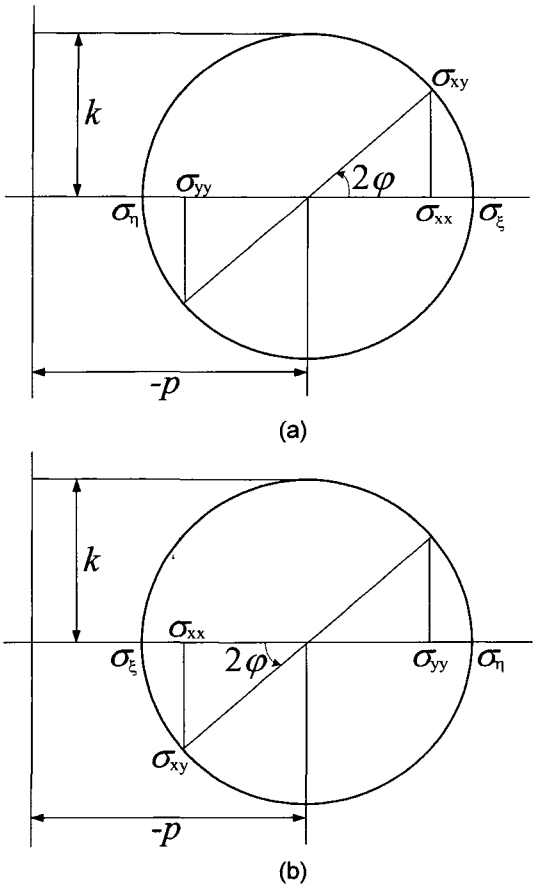

Figure 3. Yield stress status on Mohr's circle for (a) $h_\xi > h_\xi^o$ and (b) $h_\xi < h_\xi^o$.

$$p_{,\xi} \mp 2kh^2\varphi_{,\eta} = 0 \quad p_{,\eta}h^2 \mp 2k\varphi_{,\xi} = 0 \tag{16}$$

in the $\xi - \eta$ system when $\varphi = 0.0$, after considering the following inverse relationship of equation (3):

$$\xi_{,x} = \frac{1}{h}\cos\varphi \quad \xi_{,y} = \frac{1}{h}\sin\varphi \quad \eta_{,x} = -h\sin\varphi \quad \eta_{,y} = h\cos\varphi. \tag{17}$$

When φ is eliminated using equation (5), equation (16) becomes

$$\left(\frac{p}{2k} \pm \ln h\right)_{,\xi} = 0 \quad \left(\frac{p}{2k} \pm \ln h\right)_{,\eta} = 0, \tag{18}$$

therefore,

$$\frac{p}{2k} + \ln h = C^+ \quad \text{for} \quad h_\xi > h_\xi^o$$
$$\frac{p}{2k} - \ln h = C^- \quad \text{for} \quad h_\xi > h_\xi^o. \tag{19}$$

where C^+ and C^- are arbitrary constants to be decided considering the boundary conditions. For the elastic dead zone in which there is no deformation (i.e., $h_\xi = h_\xi^o$), the stress state is not unique within the yield stress surface so that the consideration of the equilibrium condition becomes involved if the dead zone is included in designing. Further discussions for such cases are referred to the work by Chung *et al.*[18].

Final Shape (Prescribed)

The real-part geometry to be formed is shown in Figure 4, which is symmetric with respect to the y-axis. Here, the boundary contours are supposed to match with materially embedded principal lines so as not have frictional boundary tractions. To apply the ideal forming for this part, this final part shape should comply with the kinematic condition discussed in equation (5). Therefore, when h and φ are

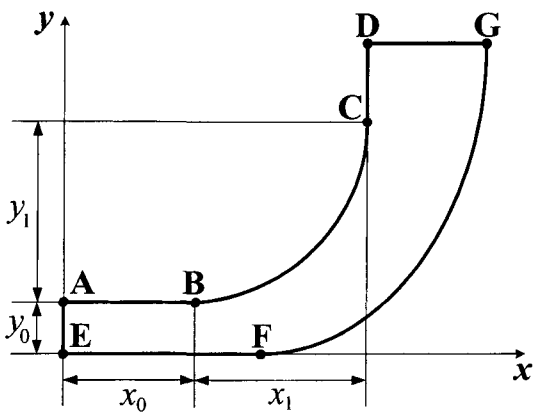

Figure 4. Schematic geometry of a real-part prescribed for ideal forming design.

properly prescribed along the line ABCD (the ξ-line with $\eta = 0$), the line EFG should be obtained from equation (5) as one of the ξ-lines. For this particular part, the analytic solution of equation (5) was available and the solution provides the following parametric expressions for the boundary contours[19]: $x = 0$ for AE, $y = 0$ for EF, $y = y_0$ for AB, $x = x_0 + x_1$ for CD, $y = y_1 + y_0(1 + e^{\pi/2})$ for DG, while

$$\left.\begin{aligned} x(\theta) &= x_0 + x_1^2 \frac{\tan\theta}{y_1 d(\theta)} \\ y(\theta) &= y_0 + y_1\left(1 - \frac{1}{d(\theta)}\right) \end{aligned}\right\} \quad \text{for BC} \tag{20}$$

$$\left.\begin{aligned} x(\theta) &= x_0 + x_1^2 \frac{\tan\theta}{y_1 d(\theta)} + e^{\theta - r_0}\sqrt{y_0}(\cos\theta + \sin\theta) \\ y(\theta) &= y_0 + y_1\left(1 - \frac{1}{d(\theta)}\right) - e^{\theta - r_0}\sqrt{y_0}(\cos\theta - \sin\theta) \end{aligned}\right\} \quad \text{for FG} \tag{21}$$

where $0 \le \theta \le \pi/2$ and $d(\theta) = (1 + (x_1 \tan\theta / y_1)^2)^{0.5}$. Here, x_0, x_1, y_0, y_1, and $r_0 (= -\ln\sqrt{y_0})$ are constants describing the part geometry shown in Figure 4: $x_0 = 1.0239$, $x_1 = 0.553$, $y_0 = 0.0264$, $y_1 = 0.9083$.

From equation (20),

$$x(\theta)_{,\theta} = \frac{x_1^2 \sec^2\theta}{y_1 d^3(\theta)} \qquad y(\theta)_{,\theta} = \frac{x_1^2 \tan\theta \sec^2\theta}{y_1 d^3(\theta)} = \tan\theta\, x(\theta)_{,\theta}, \tag{22}$$

which verifies that θ is equivalent to φ, the angle between the tangential direction of the ξ-line with the x-axis. The same procedure for equation (21) also shows the same.

Along the line ABCD, h value is also prescribed as

$$h = \frac{e^{-\theta}}{y_0}. \tag{23}$$

In order to obtain the relationship between ξ and $\theta(=\varphi)$ for the line BC, consider

$$h = l_{,\xi} \tag{24}$$

where l is the arc length along the line BC. Therefore, the relationship becomes

$$\Delta\xi(\theta = \varphi) = \int_0^\theta \xi_{,\theta} d\theta = \int_0^\theta \frac{l_{,\theta}}{h(\theta)} d\theta = \frac{x_1^2}{y_1}\int_0^\theta \frac{\sec^3\theta}{h(\theta) d^3(\theta)} d\theta. \tag{25}$$

From equations (23) and (25), $\varphi(\xi)$ and $h(\xi)$ on the line BC are obtained. Similarly,

$$\begin{aligned} \Delta\xi &= y_0 \Delta x \quad \varphi = 0 \quad \text{for AB} \\ \Delta\xi &= y_0 e^{\frac{\pi}{2}} \Delta y \quad \varphi = \frac{\pi}{2} \quad \text{for CD} \end{aligned} \tag{26}$$

The $\varphi(\xi)$ and $h(\xi)$ values on the line ABCD obtained from equations (23)-(26) provide the boundary conditions to construct the orthogonal convective coordinate system (therefore, the final part configuration) using the numerical scheme based on the characteristic method. Figure 5 shows the variation of $h(\xi)$ along the lines ABCD and EFG.

The numerically obtained final part shape agrees well with the one obtained from the parametric expressions in Figure 6, confirming the validity of the numerical method. The characteristic lines generated for the numerical solution are

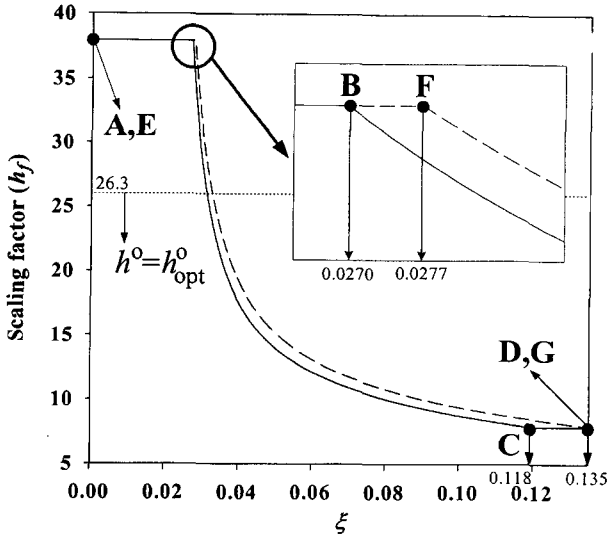

Figure 5. The distribution of the scaling factor h^f along the boundary lines ABCD and EFG on the final shape.

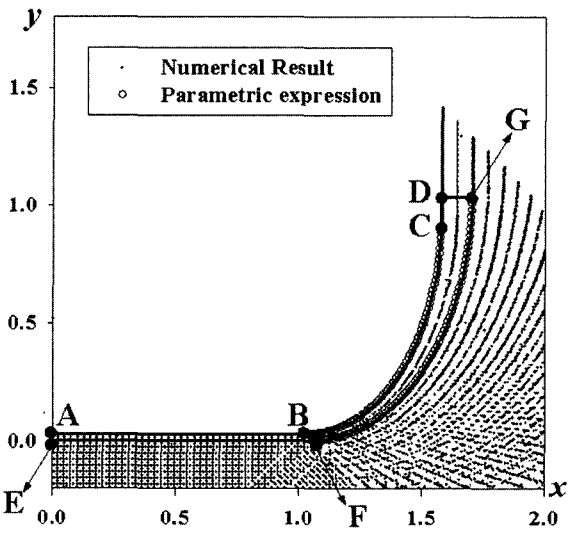

Figure 6. The principal line coordinate system numerically and analytically obtained to describe the prescribed final part.

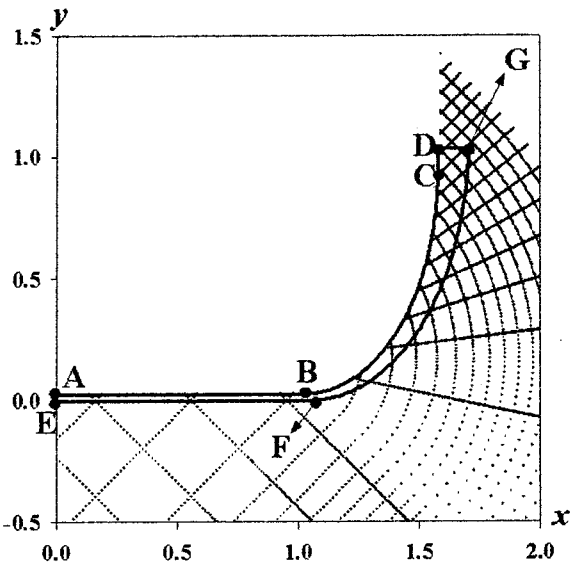

Figure 7. Characteristic lines.

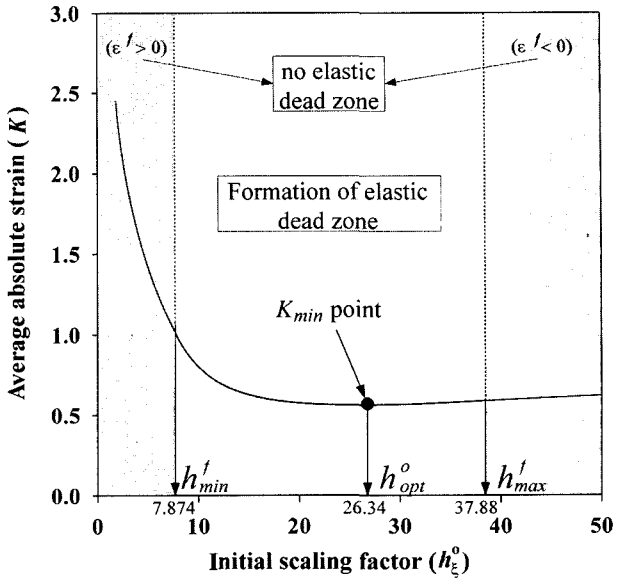

Figure 8. The average absolute strain (K) with respect to the initial scaling factor (h_ξ^o).

also plotted in Figure 7.

Optimum Initial Shape

Among many possible families to define the initial shape, a family of rectangular shapes with a uniform local scaling factor, $h_\xi^o (\equiv h^o)$, was considered here for simplicity. Also, as an optimization criterion for the initial shape, the condition of the minimum average absolute strain was considered.

The average absolute strain K is defined as

$$K = \frac{\int |\varepsilon| dA}{A}. \tag{27}$$

In equation (27), $\varepsilon = \ln(h^f/h^o)$ where the superscripts f and o refer to the final and initial configurations, respectively, while A is the total cross-sectional area of the part on the $x-y$ plane. Therefore, the following condition provides the optimum h^o:

$$\frac{dK}{dh^o} = 0. \tag{28}$$

The width of the initial shape W^o is then obtained considering the definition of the scaling factor h; i.e.,

$$W^o = \int h^o d\xi = h^o \left| \xi^{DG} - \xi^{AE} \right|. \tag{29}$$

where ξ^{DG} and ξ^{AE} are ξ values at the η lines, DG and AE, respectively. Also, the initial thickness T^o is obtained from the incompressibility condition: $T^o = A/W^o$.

The average absolute strain K as a function of the uniform initial scaling factor h^o is plotted in Figure 8. The figure shows that the minimum K is obtained for $h^o (\equiv h^o_{opt}) = 26.3$. The initial shape obtained from this optimum h^o is shown in

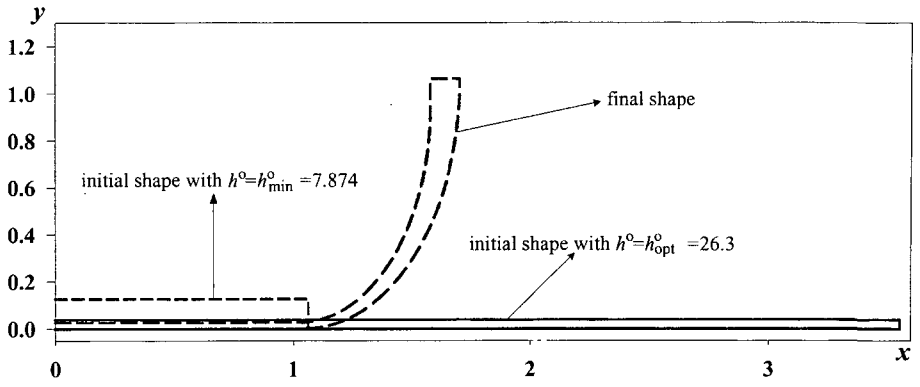

Figure 9. The initial and final shapes.

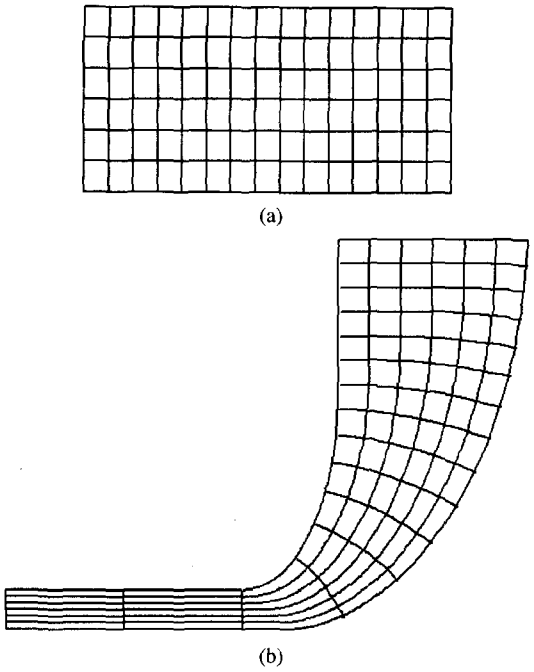

Figure 10. Schematic view of the orthogonal convective coordinate system for (a) the optimum initial and (b) final shapes.

Figure 9: $W^o = 3.56$ and $T^o = 0.038$. Schematic view of the orthogonal convective systems for the optimum initial and final shapes are shown in Figure 10. When the principal strain along the ξ lines is calculated based on the scaling factor h values in the initial and final configurations, the whole final part is divided into two zones as Figure 6 suggests: the one with the positive strain and the other with the negative strain. Therefore, for this particular part, the optimum initial rectangle introduces the elastic dead zone (or line in this case) in the middle of the part, which might require internal friction along this line to satisfy the equilibrium condition.

With the following choice of the initial scaling factor, formation of the elastic dead line in the middle of the part can be avoided:

$$\begin{aligned} h^o &< h^f_{\min}(=7.874) \quad \text{for which } \varepsilon^f > 0 \\ h^o &> h^f_{\max}(=37.88) \quad \text{for which } \varepsilon^f < 0 \end{aligned} \tag{30}$$

where the subscripts *min* and *max* refer to the minimum and maximum values, respectively. Figure 8 suggests that the average absolute strain becomes minimum as the initial scaling factor approaches to $h^f_{\min}$ or $h^f_{\max}$ when the elastic dead zone is not allowed.

Evolution of Shapes and Boundary Tractions

After the optimum initial shape was obtained, the series of intermediate shapes and frictionless external boundary tractions were subsequently calculated. Assuming that the boundary conditions for the geometric variables, h and φ, proportionally vary, the following conditions were imposed for the principal line, $\eta = 0$, to calculate intermediate shapes:

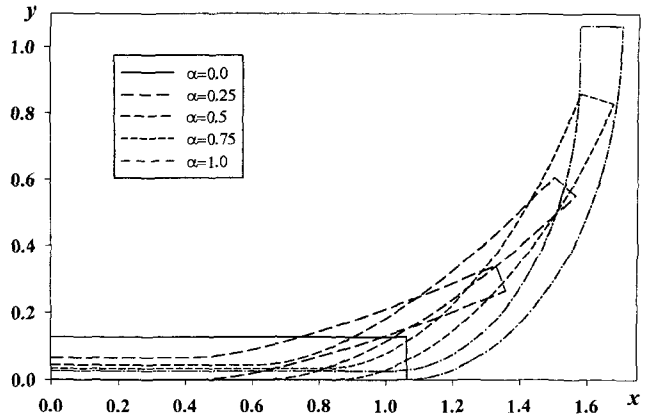

Figure 11. Evolution of the part shape when $h^o = h^o_{min}$.

$$\begin{aligned} h(\alpha) &= \alpha h^f + (1-\alpha)h^o \\ \varphi(\alpha) &= \alpha\varphi^f + (1-\alpha)\varphi^o \end{aligned} \tag{31}$$

where $0.0 \le \alpha \le 1.0$ (α varies from 0.0 to 1.0, which represents the initial and the final shapes, respectively). For demonstration purposes, only the case with $h_o = h^f_{\min}$ is considered here and the shape evolution obtained for $\alpha = 0.0, 0.25, 0.5, 0.75, 1.0$ is shown in Figure 11.

For the case with $h^o = h^f_{\min}$, the intermediate shapes obtained under the condition imposed by equation (31) provide that $\varepsilon_\xi \ge 0$ everywhere during the whole process. Therefore, equation (19-1) is applied along with the stress state shown in Figure 3(a) for the calculation of the evolving frictionless boundary tractions. When the traction-free condition is further required on the line DG, the following relationship is obtained from equation (19-1):

$$C^+ = \frac{1}{2} + \ln h^{DG}. \tag{32}$$

Note that h^{DG} is constant along the boundary line DG during forming so that the traction-free condition is allowed for the whole boundary line DG.

For the symmetric boundary line AE, the normalized stress traction becomes,

$$\tilde{\sigma}^{AE}_\xi \left(\equiv \frac{\sigma^{AE}_\xi}{k} \right) = \frac{-p^{AE}}{k} + 1 = 2\ln\frac{h^{AE}}{h^{DG}}, \tag{33}$$

which is uniform. Similarly, along the ξ-lines, including the two boundary lines, ABCD and EFG,

$$\tilde{\sigma}_\xi \left(\equiv \frac{\sigma_\xi}{k} \right) = \frac{-p}{k} + 1 = 2\ln\frac{h}{h^{DG}} \tag{34}$$

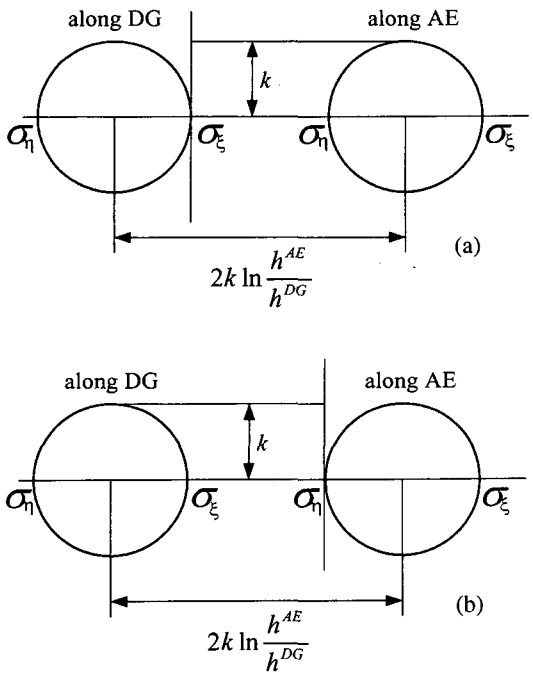

Figure 12. Mohrs circle for the stress status on the line AE and DG when (a) traction is free on the line DG and (b) boundary tractions are all negative.

where h is the value on those boundary lines. Therefore, the normalized boundary tractions on the lines ABCD and EFG become,

$$\tilde{\sigma}_\eta = \frac{-p}{k} - 1 = 2\left(\ln\frac{h}{h^{DG}} - 1\right). \tag{35}$$

The stress state along the lines DG and AE, expressed using Mohr's circles, is schematically shown in Figure 12(a). The figure shows that the tensile boundary traction (positive σ_η) is needed when the traction-free condition is imposed on the boundary DG.

Since arbitrary hydraulic pressure can be added for incompressible plasticity, the case with compressive boundary tractions only can be achieved by uniformly adding pressure. One of possible cases is obtained when $\sigma_\eta^{AE} = 0$ (therefore, $\sigma_\xi^{AE} = 2k$) as shown in Figure 12(b). For such a case,

$$\tilde{\sigma}_\xi = 2\left(\ln\frac{h}{h^{AE}} + 1\right), \qquad \tilde{\sigma}_\eta = 2\ln\frac{h}{h^{AE}} \tag{36}$$

along the ξ-lines lines, including the lines, ABCD and EFG. So that the boundary traction along the DG becomes

$$\tilde{\sigma}_\xi^{DG} = 2\left(\ln\frac{h^{DG}}{h^{AE}} + 1\right). \tag{37}$$

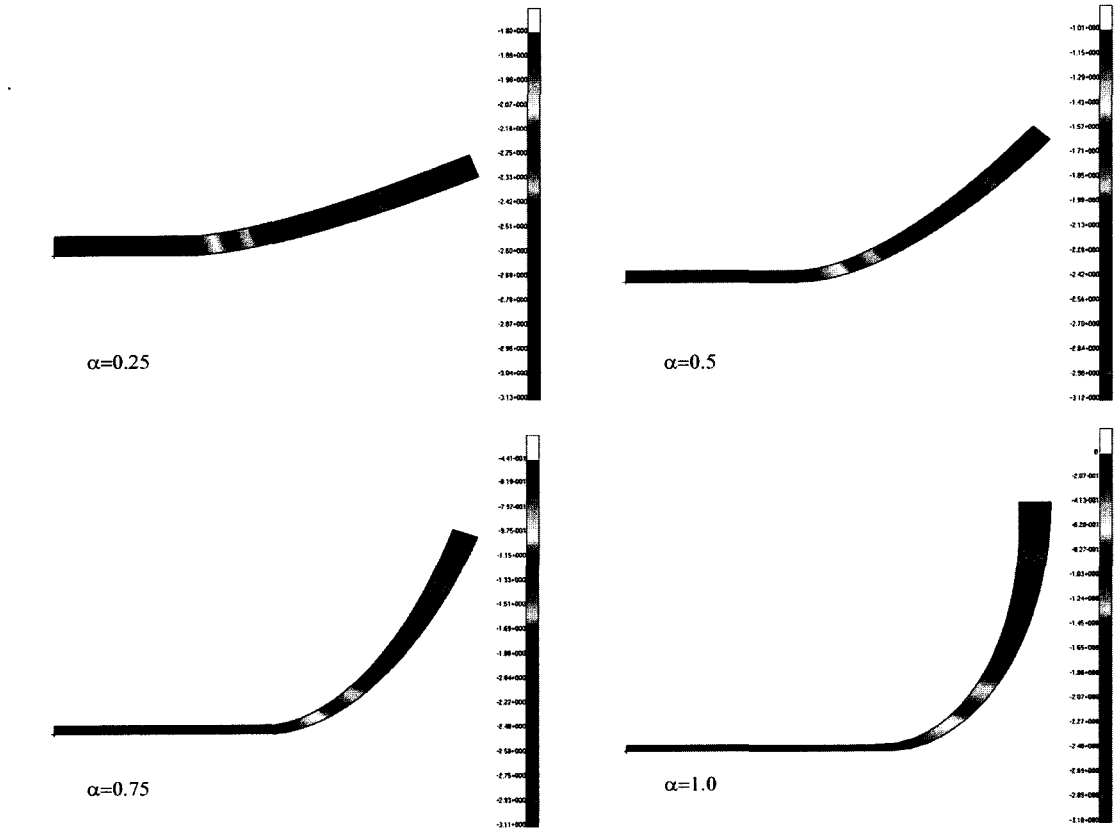

Figure 13. Normalized stress ($\tilde{\sigma}_\eta$) distribution.

The variation of $\tilde{\sigma}_\eta$ is shown in Figure 13 for $\alpha = 0.25$, 0.5, 0.75, 1.0.

Summary

The ideal forming theory, previously developed for process design purposes, was successfully applied for a non-steady plane-strain case. The minimum plastic work path, which is the kinematical constraint for ideal flow, was well accounted for using the orthogonal convective coordinate system having uniform local area. Besides kinematics, the equilibrium condition, schemes to optimize preform shapes for a prescribed final part shape and also to define the evolution of shapes and frictionless boundary tractions were developed. Numerical solutions were obtained for a real part under forging for demonstration purposes.

Acknowledgement

The authors would like to thank Drs. Sergei Alexandrov and Paul Wang for sharing the example data and also for their discussions. This work was supported by the Ministry of Science and Technology in Korea through the National Research Laboratory for which the authors feel so thankful.

References

1. O. Richmond and M. L. Devenpeck, *Proc. 4th U.S. Natn. Cong. Appl. Mech.*, 1053 (1962).
2. O. Richmond and H. L. Morrison, *J. Mech. Phys. Solids*, **15**, 195 (1967).
3. O. Richmond, *Mechanics of Solid State*, Univ. of Toronto Press, 154 (1968).
4. R. Hill, *J. Mech. Phys. Solids*, **15**, 223 (1967).
5. H. A. Wienecke and O. Richmond, *J. Appl. Mech.*, (accepted).
6. K. Chung and O. Richmond, *J. Appl. Mech.*, **61**, 176 (1994).
7. K. Chung and O. Richmond, *Int. J. Plasticity*, **9**, 907 (1993).
8. K. Chung and O. Richmond, *Int. J. Mech. Sci.*, **34**, 617 (1992).
9. F. Barlat, K. Chung, and O. Richmond, *Metallurgical and Materials Trans.*, **25A**, 1209 (1994).
10. K. Chung, F. Barlat, J. C. Brem, D. J. Lege, and O. Richmond, *Int. J. Mech. Sci.*, **39**, 105 (1997).
11. O. Richmond and K. Chung, *Int. J. Mech. Sci.*, **42**, 2455 (2000).
12. K. Chung, J. W. Yoon, and O. Richmond, *Int. J. Plasticity*, **16**, 595 (2000).
13. A. Nadai, "Theory of Flow and Fracture of Solids", Vol. 2, pp.96, McGraw-Hill, New York, 1963.
14. R. Hill, *J. Mech. Phys. Solids*, **34**, 511 (1986).
15. K. Chung and O. Richmond, *Int. J. Mech. Sci.*, **34**, 575 (1992).
16. O. Richmond and S. Alexandrov, *J. Mech. Phys. Solids*, **48**, 1735 (2000).
17. K. Chung, W. Lee, and W. R.Yu, *J. Korean Fiber Soc.*, **39**, 407 (2002).
18. K. Chung, W. Lee, and O. Richmond, *Int. J. Plasticity*, (submitted).
19. S. Alexandrov, private communication, (2001).